Faraday Discussions

Bimolecular Collision Outcomes on Multidimensional Potential Energy Surfaces: Infrared Spectroscopy and Activation of NO-Alkane Collision Complexes

Journal:	*Faraday Discussions*
Manuscript ID	FD-ART-12-2023-000176.R1
Article Type:	Paper
Date Submitted by the Author:	14-Feb-2024
Complete List of Authors:	Davis, John; College of William And Mary Department of Chemistry Burroughs, P.; College of William And Mary Department of Chemistry Wilkinson, W.; College of William And Mary Department of Chemistry Majumdar, Ellora; College of William And Mary Department of Chemistry Kidwell, Nathanael; College of William And Mary Department of Chemistry,

Bimolecular Collision Outcomes on Multidimensional Potential Energy Surfaces: Infrared Spectroscopy and Activation of NO-Alkane Collision Complexes

John P. Davis, P. Garrett Burroughs, W. Churchill Wilkinson, Ellora Majumdar, Nathanael M. Kidwell*

Department of Chemistry, The College of William & Mary, Williamsburg, VA 23187-8795, USA

Abstract

In bimolecular collisions between open-shell radicals and increasingly-larger alkanes, the relative impact configurations open the possibility to reactive and nonreactive outcomes that are isomer specific. To model the interaction potential between molecular scattering partners, observables are needed from experiments that can quantify both the initial molecular orientations and internal energies on multidimensional potential energy surfaces. Recent work by our group demonstrated that upon infrared (IR) excitation, the dynamics of the nitric oxide-methane collision complex (NO-CH_4) are dependent on the initial monomer geometries, as small changes in configuration substantially affect the energies, electronic couplings, and predissociation pathways due to the Jahn-Teller effect. This study focuses on the isomer-specific scattering mechanisms between NO and ethane (C_2H_6), encoded in the spectroscopic and dynamical signatures of the NO-C_2H_6 collision complex. IR action spectroscopy with 1+1 resonance-enhanced multiphoton ionization of NO products was employed to characterize the fundamental CH stretch transitions of NO-C_2H_6 as well as to initiate the nonreactive decay mechanisms of the complex. Furthermore, velocity map imaging (VMI) was utilized to explore the dynamics prior to and following IR excitation of NO-C_2H_6, imprinted on the NO photoproducts. This work compares the dynamics from NO-C_2H_6 and NO-CH_4 vibrational predissociation, in which substantial differences are observed in the energy exchange mechanisms during the evolution of the collision complexes to products.

*corresponding author email: nmkidwell@wm.edu

Introduction

Nitric oxide (NO) and alkanes undergo bimolecular collisions in a range of environments, including combustion and the atmosphere. In the troposphere, the anthropogenic emissions of NO and alkanes contribute to a complex series of chemical and physical transformations which have significant effects on processes like ozone production, acid rain decomposition, and the formation of secondary particulate matter through gas/particle partitioning.[1] Indeed, the intermolecular interactions prior to collision between open- and closed-shell molecules, such as NO and alkanes, fall between full chemical bonding and van der Waals interactions.[2] Therefore, not only are these chemical systems important targets for detailed investigations, but these first few collision events are also critical to characterize due to their impact on large-scale processes.

As illustrated in Figure 1, the bimolecular collision between NO and methane (CH_4) or ethane (C_2H_6) is fundamentally interesting since the reactive and/or nonreactive outcomes are steered by the relative collision geometry of the monomers at the moment of impact. The isomer varieties available to the incipient collision complexes formed along the bimolecular collision potential energy surface increase significantly with alkane size and therefore the number of NO-alkane interaction sites. The intermolecular interaction potentials and thus the collision outcomes also depend on whether either collision partner is activated in certain degrees of freedom (e.g., vibration, rotation, and/or translation) before impact. Taken together, the conditions under which collisions take place will open or block specific chemical transformations and/or energy-exchange mechanisms. To address these challenges, researchers have prepared collision complexes with well-defined relative monomer orientations and energies to control the accessible bimolecular pathways.[3–5] In recent years, many studies have worked to unravel the spectroscopy and dynamics of the NO-CH_4 complex.[5–10] However, despite their atmospheric importance, the bimolecular collision dynamics of NO complexed with larger alkanes, such as C_2H_6, have received relatively little attention.

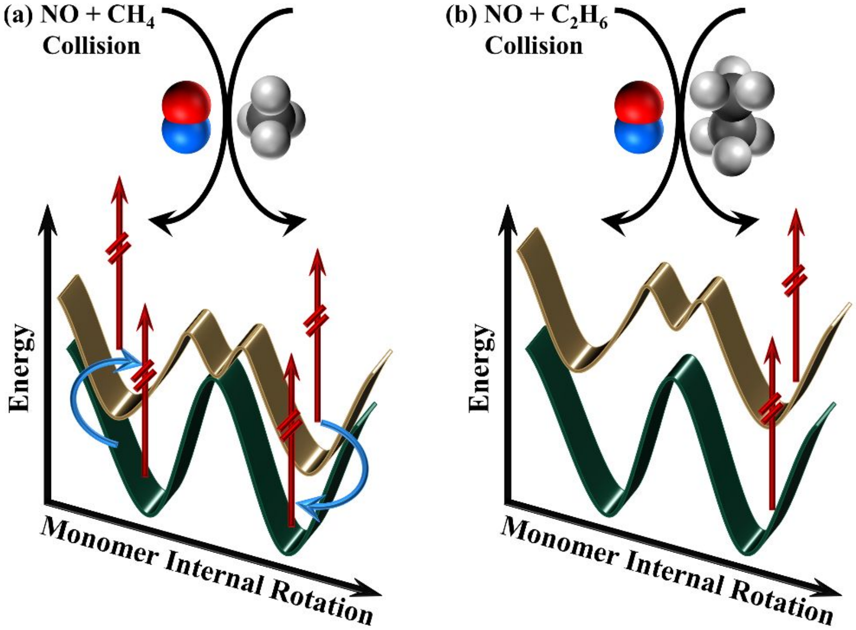

Figure 1: *Bimolecular collision between* ***(a)*** *NO + CH_4 and* ***(b)*** *NO + C_2H_6 with the incipient collision complexes formed from the intermolecular interactions between the monomers. An accompanying schematic displays the upper and lower (pseudo) Jahn−Teller potential energy surfaces from internal rotation of either monomer within each collision complex. For the NO-CH_4 collision complex, the energy difference between the Jahn-Teller surfaces may be sufficiently small to enable population interconversion (blue arrows) between surfaces, leading to four distinct population subsets that may undergo IR activation (red arrows). For the NO-C_2H_6 collision complex, the energy difference between the pseudo Jahn-Teller surfaces may be sufficiently large to prevent population interconversion between surfaces, leading to IR excitation of two unique sub-populations. The mechanisms distinguishing the two collision complexes are imprinted on the IR spectroscopy and dynamical signatures.*

Previous studies on NO-C_2H_6 have characterized the complex's vibronic spectroscopy. Wright et al. recorded the *A*-*X* transitions of NO-C_2H_6 and NO-$(C_2H_6)_2$ using (1+1) resonance-enhanced multiphoton ionization spectroscopy.[11] From the electronic spectra, the authors determined the dissociation energies of the *A* and *X* electronic states to be $D_0' = 340$ cm^{-1} and D_0''

= 190 cm^{-1}, respectively. Additionally, they observed a vibronic progression of 40 cm^{-1}, which similarly to NO-CH_4, was assigned to the intermolecular stretch of NO-C_2H_6. The electronic spectrum was partially resolved, therefore making it difficult to make full assignments in comparison with NO-CH_4.

In 2012, Wright and co-workers revisited the vibronic spectroscopy of NO-CH_4 and NO-C_2H_6, and also reported the resonance-enhanced multiphoton ionization spectra for NO-propane and NO-(*n*-butane) for the first time.[2] The UV excitation spectra for NO-CH_4 and NO-C_2H_6 were in agreement with their previous work. For NO-C_2H_6, they concluded that the isomer geometry with the lowest energy is consistent with NO aligned parallel to the C-C bond of C_2H_6 in the ground electronic state. Furthermore, they recorded the electronic spectra of larger NO-C_2H_6 complexes and their analysis revealed the relative binding energies. The initial studies of NO-C_2H_6 suggest that this weakly-bound molecular complex has complicated interactions, which make the experimental data difficult to disentangle. In contrast to NO-CH_4, the NO-C_2H_6 vibronic spectrum lacks any definitive vibronic transitions. Possible explanations included that there are more contributions, likely from greater access to a larger number of low-energy isomers and intra- and intermolecular vibrational modes.[2,8] Similar to NO-CH_4, the low-lying minima also suggest large amplitude motion of the NO-C_2H_6 complex.[2,3]

The perturbation of an alkane complexed with NO results in a splitting of the nearly degenerate $^2\Pi$ spin-orbit electronic states. Shown in Figure 1, the relative energies and symmetries of the Jahn-Teller surfaces for the NO-CH_4 complex are defined by the relative orientation of the NO π^* molecular orbital with respect to CH_4. Here, the surfaces converge at a degenerate, high-symmetry C_{3v} geometry and the complex undergoes a Jahn-Teller distortion to a lower-energy C_s configuration.[5,8] Previous theoretical work by Crespo-Otero and co-workers[8] revealed that the relative zero-point energies of NO-CH_4 are near the C_s and C_{3v} saddle points, thus increasing the likelihood that population may easily interconvert between each Jahn-Teller surface indicated with blue arrows in the figure. Therefore, the analysis of the NO-CH_4 vibrational predissociation dynamics in our previous work[5] included four main mechanisms that were differentiated by whether NO-CH_4 complexes originated on either Jahn-Teller surface or had experienced interconversion prior to IR activation (red arrows). In similar fashion, there exists two nearly isoenergetic upper and lower electronic states for the NO-C_2H_6 complex. However, a strict Jahn-Teller distortion relevant to NO-CH_4 does not apply in this situation.[2,3,8] Rather, NO-C_2H_6 likely experiences a pseudo Jahn-Teller effect, in which the upper and lower ground electronic states are separated energetically by a non-negligible degree at a high-symmetry point in the potential energy surface. As a result, the interconversion pathways present for NO-CH_4 may not be accessible for NO-C_2H_6.

The present work expands our studies on the role of Jahn-Teller dynamics prior to IR activation of NO-alkane collision complexes by increasing the alkane size from NO-CH_4 to NO-C_2H_6. Increasing the alkane chain length shifts the intermolecular interaction strength between NO and the alkane collision partner, while also tuning the coupling strength of the upper and lower (pseudo) Jahn-Teller surfaces. Therefore, we compare the vibrational predissociation dynamics between NO-CH_4 and NO-C_2H_6 to obtain new insights into bimolecular collision outcomes on multidimensional potential energy surfaces. Herein, we leverage an array of laser-based techniques to characterize the infrared spectroscopy and infrared-driven dynamics of NO-C_2H_6. Ultimately, we seek to further examine the mechanistic energy-transfer pathways prior to and following fragmentation of NO-alkane collision complexes.

Experimental Methods

A differentially-pumped molecular beam apparatus described previously[5] was employed to carry out the infrared spectroscopy and dynamics experiments. A dual flow nozzle was utilized to achieve supersonic jet expansion by pulsing a single gas flow comprised of two separate gas mixtures (1% NO/Ar and 15% C_2H_6/Ar). The total pressure was held at 2.5~3 bar and the gas mixture was ejected through a 500 μm pulse valve nozzle (Series 9, General Valve) into a high-vacuum chamber. Thereafter, NO-C_2H_6 molecular complexes were generated from adiabatic collisional cooling with the inert gas carrier. To select the NO-C_2H_6 molecular complexes with the lowest internal energy from the molecular beam, a skimmer (ID:2mm, Beam Dynamics) was positioned approximately 30 mm from the pulse valve nozzle. The NO-C_2H_6 complexes were then characterized downstream with several laser-based methods. A Nd:YAG-pumped dye laser (Radiant Dyes, NarrowScan, 10 Hz) in tandem with a set of BBO crystals produced ultraviolet (UV) radiation to detect NO-C_2H_6 molecular complexes or NO fragments following dissociation of the complex. Furthermore, tunable IR radiation was generated with an optical parametric oscillator/amplifier (OPO/OPA, LaserVision), which was pumped by another Nd:YAG laser (Continuum Surelite II-10, 5 Hz). The spatially overlapped IR and UV beams were aligned perpendicular to the molecular beam and both laser pulses were vertically polarized in the plane of the detector.

IR action spectroscopy was carried out by fixing the UV probe laser resonant on specific rovibrational transitions of NO ($X^2\Pi$, $v''=0$, J'', F_n, Λ) fragments generated from vibrational predissociation of the NO-C_2H_6 molecular complex while scanning the IR pump laser across the CH stretch region (2850-3050 cm^{-1}). The UV wavelengths were verified with a wavelength meter (Coherent WaveMaster). The spin-orbit (F_1 and F_2) and Λ-doublet ($\Pi(A'')$ and $\Pi(A')$) levels were probed using the $Q_1(J'')$, $R_1(J'')$, $Q_2(J'')$, and $R_2(J'')$ lines. When the tunable IR wavelength became resonant with a NO-C_2H_6 transition which causes vibrational predissociation of the complex, signal gain was observed in the NO^+ mass ion channel using active baseline subtraction and averaged as a function of the IR wavelength. Thus, IR action spectroscopy served as the basis for subsequent velocity map imaging (VMI) experiments.

VMI experiments were performed under the same experimental conditions to reveal the vibrational predissociation outcomes following IR activation of NO-C_2H_6 molecular complexes. Following IR fragmentation of NO-C_2H_6, the translational and angular distributions of NO ($X^2\Pi$, $v''=0$, J'', F_n, Λ) products were detected. The probed NO^+ ions were accelerated on axis with the supersonic jet expansion using a stack of ion optic plates and velocity-focused onto a position-sensitive multichannel plate/phosphor screen detector, which was gated for the NO^+ mass (m/z=30). The spatial ion images of the three-dimensional NO product ion cloud were captured with a charge-coupled device (CCD) camera, and the ion images were collected in an active baseline fashion. The resonant IR activation wavelengths were varied based on different prominent features in the IR action spectrum. Using the pBASEX[12] program, 3D ion image reconstruction was carried out to extract the anisotropy parameter, β, across the main features in the ion images. Furthermore, the ion images were analyzed with pBASEX to determine the velocity distributions of NO ($X^2\Pi$, $v''=0$, J'', F_n, Λ) products by implementing an inverse Abel transformation along the vertical axis and subsequently integrating the radial distributions over the polar angle. Using conservation of momentum, the total kinetic energy release (TKER) distributions to NO + C_2H_6 were obtained.

Results and Discussion

A. Infrared Spectroscopy of NO-Alkanes

The IR action spectra of NO-CH_4 and NO-C_2H_6 collision complexes in the CH stretch region are shown in left panel of Figure 2. In separate experiments, IR activation of either NO-CH_4 or NO-C_2H_6 led to NO products that were monitored as a function of the IR wavelength. In particular, while scanning the IR pump laser over approximately 2800-3200 cm^{-1}, the UV probe laser detected the formation of NO ($X^2\Pi$, $v''=0$, $R_1(J''=10.5)$) fragments. As seen in Figure 2 and discussed in more detail in our previous work,[5] the vibrational band origin for the asymmetric CH stretch of NO-CH_4 is located at ~3030 cm^{-1} and is significantly broadened, likely due to prompt vibrational predissociation. The homogeneous broadening of the asymmetric CH stretch band was determined, leading to a vibrational predissociation lifetime of τ_{vib} ~ 200-400 fs.

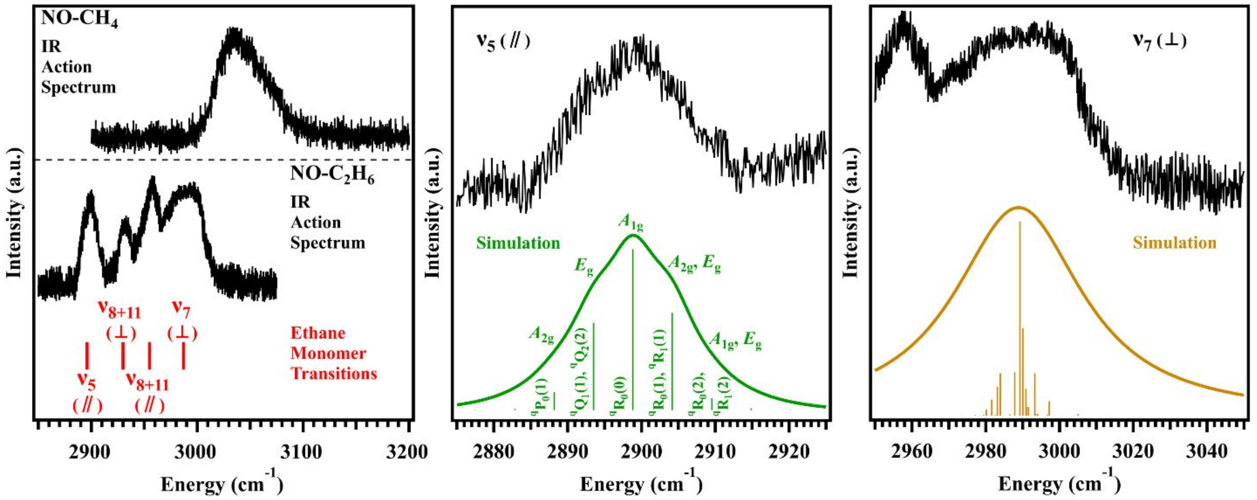

Figure 2: (Left panel) *Infrared action spectra of the NO-CH_4 and NO-C_2H_6 collision complexes (black traces) in the CH stretch region. The infrared action spectra were obtained in separate experiments with the UV probe laser fixed on the NO (A-X(0,0) R_1(10.5) product transition. The ethane monomer vibrational transition frequencies (red trace) are shown for comparison and were obtained from Ref.* 13. ***(Middel and right panels)*** *Close views of the parallel ν_5 and perpendicular ν_7 transition bands. The rovibrational simulations were obtained using the fitting procedure described in the main text and the spectroscopic constants listed in Table 1. The green and gold traces represent the fitted spectra by convoluting each stick with a Lorentzian line shape function. Transitions are labeled using the $^{\Delta K}\Delta J_{K''}(J'')$ notation along with the A_{1g}, A_{2g}, or E_g nuclear spin isomer assignments. The NO-CH_4 IR spectrum in the left panel is adapted with permission from Davis et al, J. Phys. Chem. A, 2023,* ***127****, 5171. Copyright 2023 American Chemical Society.*

Directly under the IR action spectrum of NO-CH_4 in the left panel of Figure 2 is the corresponding spectrum for the NO-C_2H_6 collision complex at lower energy, featuring an array of closely-lying vibrational bands. The gas-phase ethane monomer vibrational frequencies[13–15] are superimposed on the results as red sticks with arbitrary intensity in the lower portion of the figure. Between 2850 – 3200 cm^{-1}, the frequencies of the NO-C_2H_6 complex compared to those of the C_2H_6 monomer all exhibit shifts under ~3 cm^{-1}. We thus assign the NO-C_2H_6 spectrum based on the gas-phase C_2H_6 monomer, in which Figure 3 illustrates the vibrational modes relevant to the analysis. NO is removed from Figure 3 for simplicity since the vibrational mode nuclear displacements of NO-C_2H_6 and C_2H_6 are similar. The NO-C_2H_6 transition at 2900 cm^{-1} is assigned as the parallel ν_5 (∥) transition, ascribed to the out-of-phase symmetric CH stretch mode. At 2933 and 2957 cm^{-1} are the two ν_8+ν_{11} combination bands, which are assigned as the perpendicular (⊥) and parallel (∥) transitions, respectively. Both the ν_8 and ν_{11} fundamental bands are asymmetric methyl deformation modes. Lastly, the broadened band at ~2996 cm^{-1} is assigned to the perpendicular ν_7 (⊥) transition, with nuclear displacement involving the in-phase asymmetric CH stretch. The IR action spectra of NO-CH_4 and NO-C_2H_6 were unchanged when monitoring different NO product rotational levels.

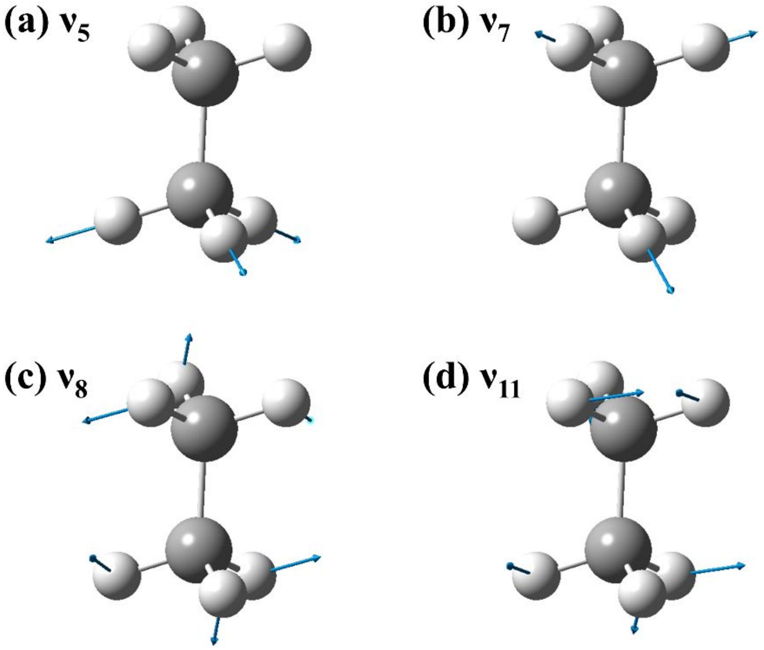

Figure 3: *Calculated vibrational modes of C_2H_6 at the DFT ωB97X-D/6-311+g(d,p) level of theory. The nuclear displacement vectors are indicated with blue arrows.*

The staggered configuration of the C_2H_6 monomer is a prolate symmetric top molecule under the D_{3d} point group. Furthermore, there are six equivalent nuclear spins of the hydrogen atoms, which correspond to the three nuclear spin isomers A_{1g}, A_{2g}, and E_g.[13] The rovibrational selection rules are dictated by symmetry and nuclear spin statistics, while the transition intensities report on the relative population in each of the nuclear spin isomers rotational levels ($J''_{K''}$). Since the NO-C_2H_6 collision complexes were generated in the cold environment of a pulsed molecular beam, it is anticipated that their formation is principally derived from monomers of NO ($X^2\Pi_{1/2}$, J''=0.5) and the C_2H_6 nuclear spin isomers in the supersonic jet expansion. The nuclear spin statistical weights of the C_2H_6 ($J''_{K''}$) levels are 8 for J'' even, K'' = 0; 16 for J'' odd, K'' = 0; 20 for K'' = 3n ± 1; and 24 for K'' = 3n ≠ 0. The relative NO-C_2H_6 ($J''_{K''}$) population ratio should reflect the predicted statistical weights, which for the A_{1g} ($J''_{K''} = 0_0$), A_{2g} ($J''_{K''} = 1_0$), and E_g ($J''_{K''} = 1_1$) nuclear spin isomers of C_2H_6 is expected to be 8:16:39.5, respectively. Interconversion between rotational levels of the C_2H_6 monomer with different nuclear spin symmetry is not anticipated on the experimental timescale of the molecular beam (~ few μs), leading to the $A_{1g} \leftrightarrow A_{1g}$, $A_{2g} \leftrightarrow A_{2g}$, and $E_g \leftrightarrow E_g$ selection rule for nuclear spin isomer transitions. Furthermore, the selection rules for rovibrational excitation have implications on the allowed nuclear spin isomer transitions.

A closer view of the ν_5 (‖) transition from IR action spectroscopy is shown in the middle panel of Figure 2, along with a rovibrational band simulation using PGOPHER.[16] To obtain the best fit to the experimental results, the ν_5 (‖) transition with a_{2u} symmetry in the D_{3d} point group was simulated as the out-of-phase symmetric CH stretch of NO-C_2H_6 initially using the spectroscopic constants for the ethane monomer from Hepp and co-workers.[13] The best-fit constants along with their respective uncertainties are listed in Table 1. The simulated rovibrational transitions shown as green sticks in the figure are labeled using notation consistent with a prolate symmetric top, ${}^{\Delta K}\Delta J_{K''}(J'')$ and are also assigned to the nuclear spin isomers. A Lorentzian line shape function ($\Delta\nu_{Lor}$) was incorporated as a fitting parameter in the simulation procedure to obtain excellent agreement with the homogeneous linewidth of the ν_5 (‖) band in the IR action spectrum.

The homogeneous broadening of the ν_5 (‖) band was found to have an upper limit of ~9 cm^{-1}. Therefore, the vibrational predissociation lifetime of the NO-C_2H_6 complex was determined to be τ_{vib} ~ 590 fs. Similar to the gas-phase[13] and helium nanodroplet[17] studies of the C_2H_6 monomer, the parallel ν_5 and ν_8+ν_{11} bands in Figure 2 are more narrow, while the perpendicular ν_8+ν_{11} and ν_7 transitions have full-width at half-maxima (FWHM) that are somewhat larger. In particular, the vibrational predissociation lifetime of the ν_7 band is shorter, as we discuss in more detail in the following paragraph.

Table 1. Fitting Parameters Obtained for the Rovibrational Simulations[a]

	ν_5 Transition	**ν_7 Transition**
Parameter	Value[b]	Value[b]
ν_0	2893.5(2)	2988.5(4)
A'' / A'	2.670(1)/2.610(1)[c]	2.670(1)/2.340(1)[c]
B'' / B'	0.663(1)/0.602(1)[c]	0.663(1)/0.645(1)[c]
$D_{J''}$	1.03x10^{-6}(1)	1.03x10^{-6}(1)
$D_{J''K''}$	2.66x10^{-6}(1)	2.66x10^{-6}(1)
$D_{K''}$	1.09x10^{-5}(1)	1.09x10^{-5}(1)
ζ	0	0.126
$\Delta\nu_{\mathrm{Lor}}$	9(1)	40(1)
T_{rot} (K)	4(1)	4(1)

[a] Standard deviations (2σ) for each parameter are given in parentheses.

[b] Otherwise indicated, units are given in wavenumbers (cm^{-1}).

[c] Ref. 13

The right panel of Figure 2 illustrates the spectral fitting results for the perpendicular ν_7 transition band with e_u symmetry in the D_{3d} point group. Here, the ν_7 band is attributed to the in-phase asymmetric CH stretch of NO-C_2H_6. The gold sticks indicate the rovibrational transitions from the simulation, which are consistent with perpendicular transitions having larger band envelops due to the additional *K''* sub-band structure. However, the FWHM of the ν_7 transition band cannot solely be accounted for using the populated rotational levels at 4 K in the simulations. Although the fitted ν_7 spectroscopic constants were similar to those for ν_5, a few notable differences include $\Delta\nu_{Lor}$ to account for the ν_7 homogeneous linewidth. Here, the homogeneous broadening of ν_7 due to prompt vibrational predissociation of the NO-C_2H_6 complex was determined to have an upper limit of 40 cm^{-1} in the simulations to obtain good agreement with the experimental IR action spectrum. The τ_{vib} of v_7 is therefore calculated to be ~ 130 fs, which is much shorter than the τ_{vib} ~ 590 fs for the v_5 band. For NO-CH_4,[5] it was concluded that the asymmetric CH stretch was more directly coupled to the intermolecular dissociation coordinate compared with the NO overtone stretch[18] due to the significantly broader FWHM of the asymmetric CH stretch transition, which correlates to a much shorter vibrational predissociation lifetime of the complex. In similar fashion, the in-phase asymmetric CH stretch (ν_7) of NO-C_2H_6 at 2996 cm^{-1} also appears to be more strongly coupled to the dissociation of the complex than the out-of-phase symmetric CH stretch (ν_5) at 2900 cm^{-1}. However, the ν_5 mode is still moderately coupled to the reaction coordinate, albeit to a lesser extent than the ν_7 mode, since the vibrational predissociation lifetime of ν_5 (τ_{vib} ~ 590 fs) is relatively short compared to the rotational period ($\tau_{rot} < 3.5$ ps) of NO-C_2H_6 determined from calculated rotational constants. The focus of the next section will be to explore the vibrational activation of NO-C_2H_6 complexes to reveal the dynamics of energy partitioning to products.

B. Infrared-Driven Dynamics of NO-C_2H_6

As seen in the IR action spectrum of NO-C_2H_6 in Figure 2, there are a multitude of prominent peaks which correspond to a variety of IR activation energies to initiate vibrational predissociation of the NO-C_2H_6 complex. Therefore, IR activation energies of 2900 cm^{-1}, 2933 cm^{-1}, 2957 cm^{-1}, and 2996 cm^{-1} were used to carry out VMI experiments. The ion images for the NO ($X^2\Pi$, v''=0) Q_1(J''=5.5)) and R_1(J''=2.5)) product levels populated from IR photolysis of NO-C_2H_6 at 2996 cm^{-1} are shown as insets in Figure 4. The ion image results for the other three IR activation wavelengths are similar to those found for 2996 cm^{-1}. We conclude that there are not significant differences in the dynamics between these excitation wavelengths, and we therefore focus our analysis on the 2996 cm^{-1} excitation results.

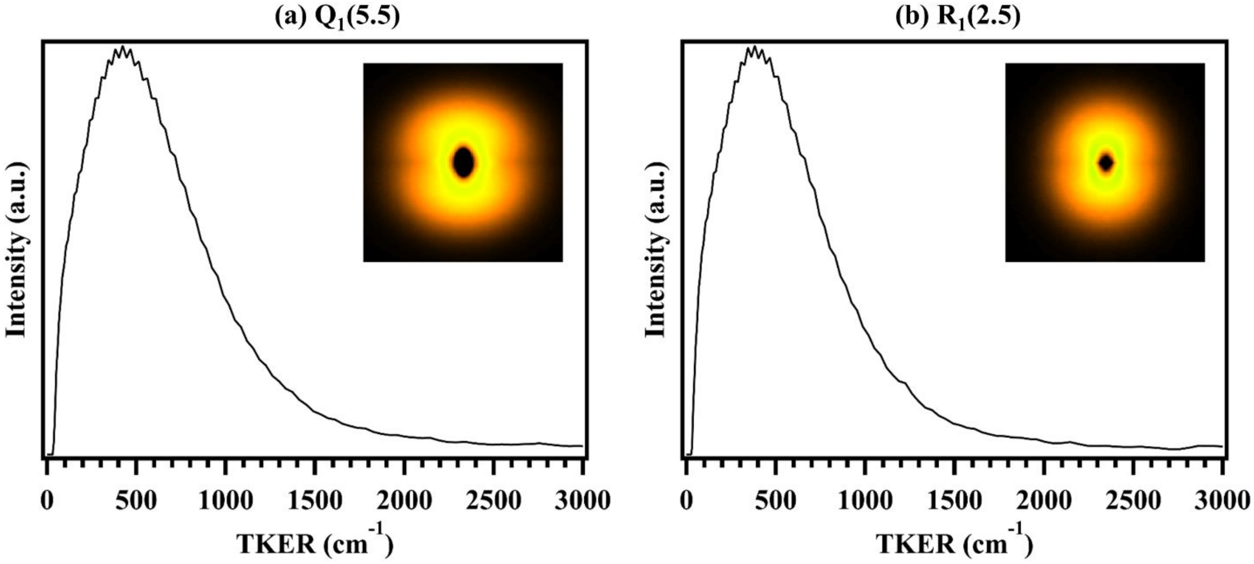

Figure 4: *TKER distributions of C_2H_6 and* ***(a)*** *NO ($X^2\Pi$, v''=0, Q_1(J''=5.5)) or* ***(b)*** *NO ($X^2\Pi$, v''=0, R_1(J''=2.5)) products using an IR activation wavelength of 2996 cm^{-1} to fragment NO-C_2H_6 complexes. The insets show the experimental ion images, revealing anisotropic ion distributions. The IR pump laser is parallel to the detector plane.*

Since vertically polarized radiation with respect to the detector plane was used during VMI experiments, the angular distribution can be extracted quantitatively from ion images by converting the laboratory frame to the molecular frame distribution using the equation, $I(\theta) = (1$

+ $\beta \bullet P_2(\cos\theta))/4\pi$. In this expression, θ is the angle between the fragment velocity vector and the vertical laser polarization, and P_2 is a second-order Legendre polynomial. The anisotropy parameter β yields information on the angular distribution of NO products in the ion image. Additionally, to determine the total kinetic energy release (TKER) distributions for NO + C_2H_6 products, the ion images were analyzed with pBASEX.[12] Employing an inverse Abel transformation of the images along the vertical axis and integrating over the polar coordinate, the TKER distributions for NO + C_2H_6 co-products using conservation of momentum are also displayed in the figure as the accompanying black traces. When monitoring the $Q_1(5.5)$ and $R_1(2.5)$ levels of NO products, the prominent features in the TKER distributions peak at ~370 and ~330 cm^{-1}, respectively, and both have a FWHM of approximately 750 cm^{-1}. Furthermore, β across the ~370 and ~330 cm^{-1} components is ~ +0.42(4) and ~ +0.38(3) on average, thus confirming the ion images are anisotropic and indicate a prompt dissociation pathway giving rise to the monitored NO products. In general, a prompt dissociation mechanism is observed only when probing low $R_1(J'')$ and $Q_1(J'')$ levels in the lower F_1 ($^2\Pi_{1/2}$) spin-orbit state of NO, whereas the $R_2(J'')$ and $Q_2(J'')$ levels in the upper F_2 ($^2\Pi_{3/2}$) spin-orbit state did not display anisotropic ion images. For the $R_1(J'')$ and $Q_1(J'')$ images, this is consistent with NO-C_2H_6 vibrational predissociation occurring on a faster timescale compared to its rotational period ($\tau_{rot} < 3.5$ ps). Additionally, these results agree with the relatively short vibrational predissociation lifetime of the ν_7 and ν_5 modes determined from the IR rovibrational spectroscopy simulations. It is instructive to first summarize the dynamical signatures from NO-CH_4 vibrational predissociation, and then we will turn the discussion to address the underlying mechanisms of the NO-C_2H_6 collision complex before and following IR activation that lead to the prompt dissociation pathway.

Derived from the two spin-orbit states ($^2\Pi_{1/2}$, $^2\Pi_{3/2}$) of NO with a 119.82 cm^{-1} energy difference,[19] the corresponding ground state potential energy surfaces of NO-CH$_4$ form Jahn-Teller surfaces which were calculated by Crespo-Otero[8] for different NO and CH$_4$ monomer orientations. Among the lowest-energy NO-CH$_4$ isomers included that with a C_{3v} geometry, whereby the O-atom of NO is pointed towards the facial H-atoms of CH$_4$ in an NO--H$_3$C-H orientation. However, an energy-stabilizing Jahn-Teller rotation within the NO-CH$_4$ complex causes the NO monomer to be perpendicular to the facial H-atoms of CH$_4$, resulting in a symmetry reduction to C_s; the upper and lower Jahn-Teller surfaces thus have A' and A'' symmetry, respectively. The spin-orbit splitting ($a\zeta_e d$) of the two Jahn-Teller surfaces when CH$_4$ combines with NO is a result of electronic and vibronic quenching.[20] The energy separation (ΔE) between the two Jahn-Teller surfaces of NO-CH$_4$ can be determined using $\Delta E = \sqrt{[(\Delta E_0)^2 + (a\zeta_e d)^2]}$, where ΔE_0 is the Jahn-Teller splitting of NO-CH$_4$. Due to the weak intermolecular interaction between the NO and CH$_4$ monomers, $a\zeta_e d$ was approximated[5] to have a lower and upper limit of 100 and 120 cm^{-1}, respectively, and the Jahn-Teller splitting was ascertained by Crespo-Otero to be ΔE_0 = 30 cm^{-1}.[8] Therefore, the ΔE for NO-CH$_4$ was calculated to be between 104 - 124 cm^{-1}. The zero-point energy of NO-CH$_4$ determined by Crespo-Otero[8] is on the same order as the calculated ΔE between the Jahn-Teller surfaces. Therefore, it is plausible that subsets of NO-CH$_4$ population with sufficient zero-point and/or rotational energy will surmount the barrier to cross between the two Jahn-Teller surfaces, thus facilitating $A' \leftrightarrow A''$ population interconversion. In our previous work on NO-CH$_4$,[5] we revealed the prompt vibrational predissociation dynamics that were imprinted on the NO product state and angular distributions. The product dynamical signatures were rationalized to result from IR activation of NO-CH$_4$ population subsets, which were differentiated by whether they originated on either A' or A'' Jahn-Teller surface or underwent $A' \leftrightarrow A''$ interconversion. We therefore assigned the $Q_1(J'')$, $R_1(J'')$, $Q_2(J'')$ and $R_2(J'')$ product states of NO ($X^2\Pi$, $v''=0$, J'', F_n, Λ) with anisotropic ion images to arise from these four pathways that are likely available prior to IR activation of NO-CH_4. The mechanistic assignments were also made by verifying that both energy and symmetry were conserved in going from NO-CH_4 complexes to NO ($X^2\Pi$, $v''=0$, J'', F_n, Λ) + CH_4 (v) product states.

Similar to NO-CH_4,[8] the ground potential energy surfaces of NO-C_2H_6 are expected to form two pseudo Jahn-Teller surfaces. Shown in the left panel of Figure 5, a schematic illustrates the pseudo Jahn-Teller potential energy surfaces of NO-C_2H_6 that were adapted from the lowest-energy NO-CH_4 isomer surfaces by Crespo-Otero.[8] However, the pseudo Jahn-Teller surfaces of NO-C_2H_6 have been energetically separated from each other, whereas the corresponding NO-CH_4 Jahn-Teller surfaces were more nearly degenerate. We approximate ΔE_0 and $a\zeta_e d$ to be a factor of two larger for NO-C_2H_6 compared to NO-CH_4 since NO interacts with each alkane through their polarizability, which is greater for C_2H_6 by a factor of two. Therefore, the ΔE between the NO-C_2H_6 pseudo Jahn-Teller surfaces is calculated with an upper limit to be ~209-257 cm^{-1}, which may be sufficiently large to prevent population interconversion between the surfaces. This may be particularly the case since the zero-point energy levels of NO-C_2H_6 isomers are likely to be somewhat lower than ΔE compared to NO-CH_4.

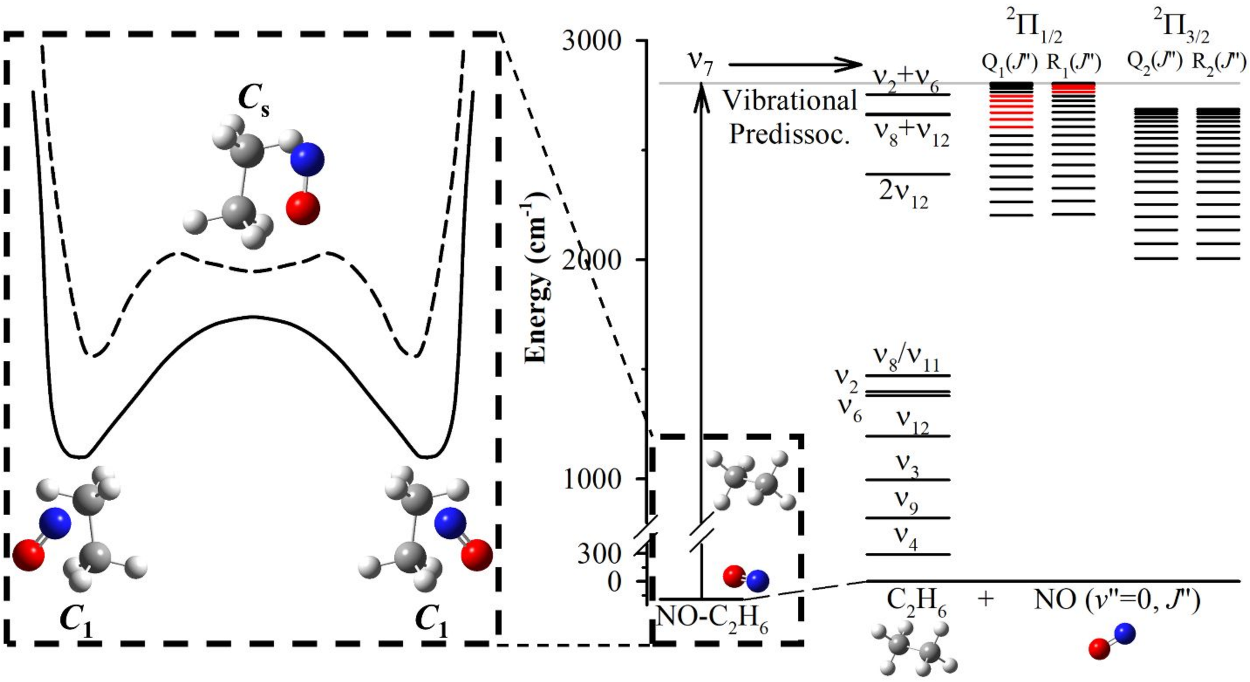

Figure 5: *Energy-level diagram illustrating the nonreactive bimolecular collision dynamics of NO−C_2H_6 complexes.* ***(Left panel)*** *Schematic of the pseudo Jahn−Teller potential energy surfaces of NO−C_2H_6 prior to IR activation. Even with sufficient zero-point and/or rotational energy, the NO−C_2H_6 complexes may not interconvert between the pseudo Jahn-Teller electronic states within the C_1 geometry or through the C_s geometry due to energy constraints.* ***(Right panel)*** *The NO−C_2H_6 complexes are prepared with one quantum in the in-phase asymmetric CH stretch (ν_7) mode indicated by the vertical black arrow. This leads to vibrational predissociation of NO-C_2H_6 to symmetry-restricted NO ($X^2\Pi$, $v''=0$, J'', F_n, Λ) + C_2H_6 (v) co-products. The energetically allowed vibrational states of C_2H_6 fragments are shown correlating with NO ($v''=0$). The allowed spin−orbit ($^2\Pi_{1/2}$, $^2\Pi_{3/2}$) and rotational levels (J'') of NO ($v''=0$) products are also shown following vibrational predissociation of NO−C_2H_6. The red NO ($X^2\Pi$, $v''=0$, J'', F_n, Λ) product levels indicate the probed states with ion images primarily displaying anisotropic angular distributions.*

In Figure 5, the lowest-energy isomer of NO-C_2H_6 determined by Tamé-Reyes[2] is shown having C_s symmetry with the N=O bond eclipsing the C-C ethane monomer bond. Indeed, this NO-C_2H_6 isomer geometry is characterized by each monomer positioned parallel to one another with the three facial H-atoms of C_2H_6 oriented towards NO. However, similar to NO-CH_4, the NO-C_2H_6 complex can undergo an energy-stabilizing pseudo Jahn-Teller distortion, in which the isomer geometry then possesses C_1 symmetry. Shown as the solid black line in the figure, the lower pseudo Jahn-Teller state of NO-C_2H_6 corresponds to the π* molecular orbital of NO lying perpendicular to the plane bisecting the C-C bond and three facial H-atoms of C_2H_6. In contrast, when the NO π* molecular orbital is parallel with this plane, the upper NO-C_2H_6 pseudo Jahn-Teller state is formed, which is portrayed as the broken black line.

Shown in the right panel of Figure 5, IR activation of NO-C_2H_6 using the in-phase asymmetric CH stretch (ν_7) at 2996 cm^{-1} will result in vibrational predissociation of the complex, with the available energy (E_{avl}) partitioned into the internal energy (E_{int}; vibrational, rotational, spin-orbit) and relative translation (TKER) of the NO and C_2H_6 products. Tamé-Reyes and co-workers[2] ascertained the intermolecular bond dissociation (D_0) of NO-C_2H_6 to be 190 cm^{-1}, yielding E_{avl} = 2806 cm^{-1}. According to the energy gap law,[21,22] it is expected that the dominant mechanism of energy exchange will be near-resonant vibration-to-vibration energy transfer from NO-C_2H_6 (ν_7) to the vibrational stretching modes of C_2H_6 and some degree of energy flow to the NO rotational levels within its $^2\Pi_{1/2}$ and $^2\Pi_{3/2}$ spin-orbit electronic states. In the figure, the C_2H_6 vibrational levels are increasing in energy from bottom to top, and the NO (v''=0) internal energy states with increasing rotational and spin-orbit energy are going from top to bottom. Below E_{avl} indicated by the grey line, there are four near-resonant C_2H_6 vibrational levels that may be populated following predissociation of NO-C_2H_6, including the $\nu_2+\nu_6$ (a_{2u}) level, the parallel and perpendicular $\nu_8+\nu_{12}$ ($a_{1u}+a_{2u}+e_u$) levels, and the $2\nu_{12}$ ($a_{1g}+a_{2g}+e_g$) level located at 2753, 2665 2660 and 2390 cm^{-1}, respectively. The NO ($X^2\Pi$, v''=0, J'', F_n, Λ) product levels highlighted red in the figure indicate the probed quantum states that displayed anisotropic ion distributions (or prompt NO-C_2H_6 dissociation) like those shown in Figure 4 when carrying out VMI experiments. The C_2H_6 vibrational levels to lower energy in Figure 5 are not likely to contribute to the prompt vibrational predissociation mechanism since they are far away from resonance (> 1300 cm^{-1}).

Figure 6 illustrates the vibrational mode nuclear displacements relevant to the $\nu_2+\nu_6$, $\nu_8+\nu_{12}$ and $2\nu_{12}$ C_2H_6 levels.

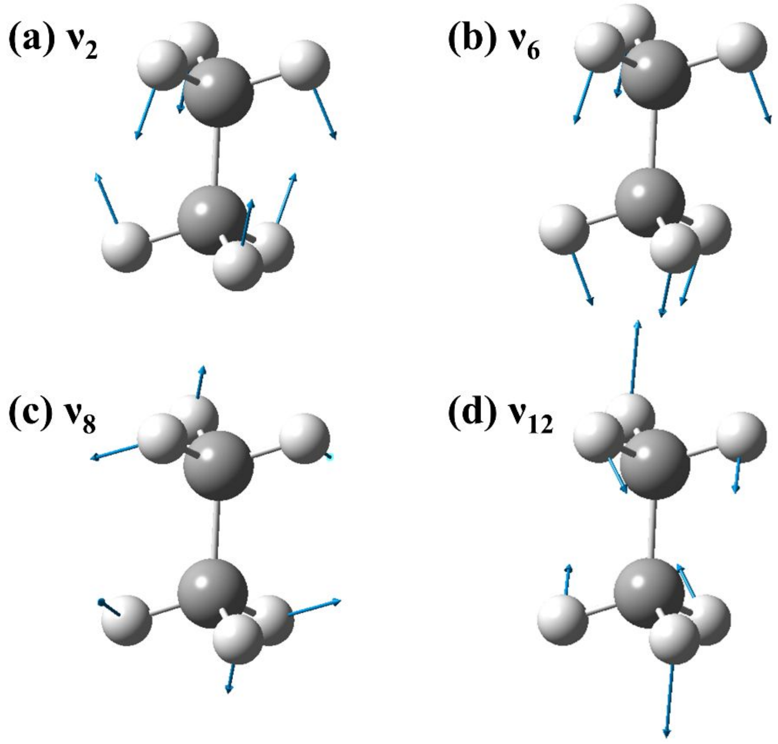

Figure 6: *Calculated vibrational modes of C_2H_6 at the DFT ωB97X-D/6-311+g(d,p) level of theory. The nuclear displacement vectors are indicated with blue arrows.*

In the absence of any external perturbations, there are two degenerate asymmetric CH stretches for the ν_7 (e_u) vibrational mode of C_2H_6. The intermolecular interaction between NO and C_2H_6 when the complex is formed breaks this double degeneracy to form two asymmetric CH stretches with calculated vibrational frequencies separated by less than 1 cm^{-1}. Therefore, for the lowest-energy NO-C_2H_6 isomer in the C_1 symmetry point group, the two asymmetric CH stretches become *a* symmetry, in which one of the vibrational modes is described as a simultaneous stretching of the three facial H-atoms of C_2H_6 and a compression of the posterior H-atoms (see Figure 3). Upon $v_7'(a)=1 \leftarrow v_7''(a)=0$ excitation of NO-C_2H_6, vibrational predissociation to products takes place, where energy may be retained in the v_2+v_6, v_8+v_{12} ($\parallel$), v_8+v_{12} ($\perp$) and/or $2v_{12}$ levels of C_2H_6 that are nearly resonant. In the case of the v_8+v_{12} ($\parallel$) state, this would leave 141 cm^{-1} of excess energy to be placed into the rotational and spin-orbit energy of NO. The red-highlighted NO ($X^2\Pi$, $v''=0$, $Q_1(J''=4.5\text{-}8.5)$ or $R_1(J''=2.5\text{-}4.5)$) states that are populated from prompt dissociation of NO-C_2H_6 spanning 13-133 cm^{-1} agree well with the excess energy available, therefore conserving energy. In addition to conservation of energy, the overall symmetry from NO-C_2H_6 reactants to NO + C_2H_6 products must also be conserved.

Based on the vibrational predissociation dynamics of NO-CH_4 discussed above and the schematic pseudo Jahn-Teller surfaces shown in Figure 5, we attribute the prompt NO-C_2H_6 dynamics to two possible mechanisms. The pathways by which NO-C_2H_6 complexes undergo vibrational predissociation are differentiated by whether a sub-population of NO-C_2H_6 originated on the upper or lower pseudo Jahn-Teller surface prior to IR activation. Furthermore, the energy separation (ΔE) between the pseudo Jahn-Teller surfaces may be reasonably large such that population on the upper and lower potential energy surface may not interconvert. Therefore, the two pathways present for NO-CH_4 that resulted from $A' \leftrightarrow A''$ Jahn-Teller state interconversion may not be accessible for NO-C_2H_6. We recorded the NO product ion images for the different spin−orbit (F_1 and F_2) and Λ-doublet ($\Pi(A'')$ and $\Pi(A')$) levels using the $Q_1(J'')$, $R_1(J'')$, $Q_2(J'')$, and $R_2(J'')$ lines. In particular, the Q-branch transitions have a high selectivity for the $\Pi(A'')$ state, whereas the $\Pi(A')$ state may be probed with the R-branch (or P-branch) transitions.[23]

First, we will consider the prompt vibrational predissociation mechanism of the NO-C_2H_6 population undergoing IR activation from the lower pseudo Jahn-Teller surface. The vibrational ground state and excited ν_7 vibrational level involving excitation of the in-phase asymmetric stretch share the same symmetry in the C_1 point group, therefore resulting in a parallel vibrational transition. This is consistent with the parallel anisotropic angular distributions ($\beta \sim +0.42$ and $\sim +0.38$) observed in the NO product ion images indicating prompt NO-C_2H_6 fragmentation. In the D_{3d} point group, the ν_7 mode has e_u symmetry. To have a shared point group convention between the reactants and products to verify symmetry conservation, we will use the D_{3d} point group for the remainder of the manuscript. Including the nuclear spin isomers with A_{1g}, A_{2g}, and E_g symmetry, the NO-C_2H_6 reactants' total symmetry from activation of the ν_7 transition involves

$$\Gamma_{elect} \otimes [\Gamma_{vib'} \otimes \Gamma_{vib''}] \otimes \Gamma_{nucl.\ spin}$$

$$= A_{1g} \otimes [e_u \otimes a_{1g}] \otimes [A_{1g}, A_{2g}, E_g]$$

$$= A_{1u} \oplus A_{2u} \oplus E_u$$

Following prompt vibrational predissociation of NO-C_2H_6 to NO ($X^2\Pi$, $v''=0$, J'', F_n, Λ) + C_2H_6 ($\nu_8+\nu_{12}$ ($\|$)) products, probing the $Q_1(J'')$ or $R_1(J'')$ transitions of NO will differentiate between A_{2g} or A_{1g} symmetries, respectively. In particular, the red-highlighted NO product levels in Figure 5 are the populated states from prompt NO-C_2H_6 vibrational predissociation. When detecting NO products using the $R_1(J'')$ spin-orbit transitions, the total symmetry of the products is

$$\Gamma_{NO} \otimes \Gamma_{C_2H_6} = A_{1g} \otimes [a_{1u} \oplus a_{2u} \oplus e_u] = A_{1u} \oplus A_{2u} \oplus E_u$$

Therefore, the total symmetry is conserved in going from NO-C_2H_6 reactants evolving to NO + C_2H_6 products. Using a similar argument, the total product symmetry is the same while probing NO($Q_1(J'')$) levels. Therefore, we tentatively assign the NO($R_1(J'')$) products to the IR activation of NO-C_2H_6 complexes originating on the lower pseudo Jahn-Teller surface since the populated J'' levels have relatively low energy. In contrast, we tentatively assign the NO-C_2H_6 complexes undergoing IR excitation from the upper pseudo Jahn-Teller surface to the NO($Q_1(J'')$) products since they occupy relatively larger J'' states. When considering which C_2H_6 levels may be populated in tandem with the NO products showing anisotropic ion images, the $\nu_2+\nu_6$ and $2\nu_{12}$ states with a_{2u} and $a_{1g}+a_{2g}+e_g$ symmetry, respectively, are not viable candidates since the total symmetry conservation requirements are not met. However, populating the $\nu_8+\nu_{12}$ ($\perp$) level of C_2H_6 cannot be ruled out as a possibility from NO-C_2H_6 predissociation. Additionally, the total symmetry between the reactants and products is also conserved when IR exciting NO-C_2H_6 complexes with the ν_5 transition.

In viewing the vibrational modes involved in the excitation of NO-C_2H_6 and the populated C_2H_6 levels, the form of the modes yields some insight into the prompt vibrational predissociation dynamics. IR activation of the in-phase asymmetric CH stretch (ν_7) of NO-C_2H_6 shown in Figure 3 involves simultaneous stretching of the facial H-atoms closest the NO collision partner and compression of the three posterior H-atoms of C_2H_6. Following prompt vibrational predissociation, the most likely C_2H_6 vibrational levels populated include the parallel and/or perpendicular $\nu_8+\nu_{12}$ states. Figure 5 illustrates the nuclear displacements of the ν_8 and ν_{12} modes, in which ν_8 is characterized as an umbrella mode of the three facial H-atoms of C_2H_6. Similarly, the $2\nu_4$ CH_4 vibrational mode occupied from NO-CH_4 vibrational predissociation[5] is also described as an umbrella mode. Therefore, both collision complexes may share analogous prompt dynamics to product formation. Additionally, the ν_{12} vibrational mode of C_2H_6 is portrayed as a buckling mode in Figure 5, which may account for the broadened TKER features in Figure 4 due to rotational excitation involving this buckling motion. By energy conservation, the translational features at ~370 and 330 cm^{-1} in the figure may correspond to either the $\nu_8+\nu_{12}$ or $2\nu_{12}$ modes of C_2H_6. However, the conservation of symmetry requirement between IR activated NO-C_2H_6 complexes and the NO + C_2H_6 co-products is only met when the ν_8+ν_{12} level of C_2H_6 is populated. Therefore, we tentatively assign the translational features to the C_2H_6 (ν_8+ν_{12}) product vibrational levels.

Conclusions

The infrared spectroscopy and infrared-driven dynamics are analyzed for the prototypical, open-shell collision complex, NO-C_2H_6, generated along the bimolecular collision pathway between NO and C_2H_6. Comparing the experimental observables of NO-C_2H_6 to the analogous results of NO-CH_4,[5] the (pseudo) Jahn-Teller dynamics taking place on multidimensional potential energy surfaces is explored. Using IR action spectroscopy in tandem with 1+1 resonance-enhanced multiphoton ionization of NO products, the fundamental CH stretch transitions belonging to the NO-C_2H_6 complex are revealed. The NO-C_2H_6 vibrational bands are negligibly shifted compared to the C_2H_6 monomer. However, the transition breadths indicate prompt decomposition of the complex due to strong coupling between the excited fundamental CH stretches and the intermolecular dissociation coordinate. From the spectral fitting procedure, the vibrational predissociation lifetime of NO-C_2H_6 was determined to be between ~130-590 fs, depending on the activated mode.

Initiating vibrational predissociation of NO-C_2H_6, the energy deposited along the CH stretches of the complex exceeds the intermolecular bond dissociation energy. Thus, the available energy is partitioned into the translational and internal energy degrees of freedom of the NO ($X^2\Pi$, $v''=0, J'', F_n, \Lambda$) + C_2H_6 (ν) co-fragments. Velocity map imaging of NO products was used to probe the pseudo Jahn-Teller dynamics before IR activation and to unravel the predissociation dynamics after vibrational excitation. The relatively few NO product rotational states populated from NO-

C_2H_6 dissociation appeared in the lower ($^2\Pi_{1/2}$) spin-orbit state, displaying anisotropic ion images that are consistent with prompt dissociation. In contrast, IR predissociation of NO-CH_4 resulted in populating NO (v''=0, J'') levels in both the upper and lower ($^2\Pi_{3/2}$, $^2\Pi_{1/2}$) spin-orbit states. Thus, this indicates significant differences in the mechanisms available to each collision complex due to the likely greater energy separation between the (pseudo) Jahn-Teller surfaces with increasing alkane size. Based on energy and symmetry conservation, the dynamical signatures from NO-C_2H_6 vibrational predissociation are rationalized between the activated modes of the C_2H_6 chromophore within the complex and the rovibrational levels of the NO and C_2H_6 co-products.

Author Contributions

JPD: investigation (experiment), writing – reviewing and editing; PGB: investigation (experiment); WCW: investigation (experiment); EM: investigation (experiment); NMK: conceptualization (experiment), supervision (experiment), analysis (experiment), writing – original draft

Conflict of Interest

There are no conflicts to declare.

Acknowledgements

NMK acknowledges support from the donors of the American Chemical Society Petroleum Research Fund (PRF# 65737-UR6) and NSF CAREER award CHE- 2239624. The authors also acknowledge William & Mary Research Computing for providing computational resources that contributed to the results reported within this paper. We gratefully acknowledge Dr. Laura McCaslin for helpful comments.

References

(1) Atkinson, R. Atmospheric Chemistry of VOCs and NO_x. *Atmos. Environ.* **2000**, *34*, 2063–2101.

(2) Tamé-Reyes, V. M.; Gardner, A. M.; Harris, J. P.; McDaniel, J.; Wright, T. G. Spectroscopy of the $\tilde{A}$ State of NO–Alkane Complexes (Alkane = Methane, Ethane, Propane, and *n* -Butane). *J. Chem. Phys.* **2012**, *137*, 214307.

(3) Wheeler, M. D.; Tsiouris, M.; Lester, M. I.; Lendvay, G. OH Vibrational Activation and Decay Dynamics of CH_4–OH Entrance Channel Complexes. *J. Chem. Phys.* **2000**, *112*, 6590–6602.

(4) Tsiouris, M.; Wheeler, M. D.; Lester, M. I. Activation of the CH Stretching Vibrations in CH_4–OH Entrance Channel Complexes: Spectroscopy and Dynamics. *J. Chem. Phys.* **2001**, *114*, 187–197.

(5) Davis, J. P.; Neisser, R. W.; Kidwell, N. M. Infrared Activated Signatures and Jahn–Teller Dynamics of NO–CH_4 Collision Complexes. *J. Phys. Chem. A 127*, 5171–5182.

(6) Musgrave, A.; Bergeron, D. E.; Wheatley, R. J.; Wright, T. G. Electronic Spectroscopy of the Deuterated Isotopomers of the NO·Methane Molecular Complex. *J. Chem. Phys.* **2005**, *123*, 204305.

(7) Akiike, M.; Tsuji, K.; Shibuya, K.; Obi, K. Van Der Waals Vibrations of NO-Methane Complexes in the $A^2\Sigma^+$ State. *Chem. Phys. Lett.* **1995**, *243*, 89–93.

(8) Crespo-Otero, R.; Suardiaz, R.; Montero, L. A.; García de la Vega, J. M. Potential Energy Surfaces and Jahn-Teller Effect on $CH_4\cdots NO$ Complexes. *J. Chem. Phys.* **2007**, *127*, 104305.

(9) Holmes-Ross, H. L.; Gascooke, J. R.; Lawrance, W. D. Correlated Product Distributions in the Photodissociation of A State NO–CH_4 and NO–N_2 van der Waals Complexes. *J. Phys. Chem. A* **2022**, *126*, 7981–7996.

(10) Wang, X.-D.; Robertson, P. A.; Cascarini, F. J. J.; Quinn, M. S.; McManus, J. W.; Orr-Ewing, A. J. Observation of Rainbows in the Rotationally Inelastic Scattering of NO with CH_4. *J. Phys. Chem. A* **2019**, *123*, 7758–7767.

(11) Daire, S. E.; Lozeille, J.; Gamblin, S. D.; Wright, T. G. The $\tilde{A} \leftarrow \tilde{X}$ (1 + 1) Resonance-Enhanced Multiphoton Ionization Spectrum of the $NO\cdot C_2H_6$ and $NO\cdot(C_2H_6)_2$ Complexes. *J. Phys. Chem. A* **2000**, *104*, 9180–9183.

(12) Dribinski, V.; Ossadtchi, A.; Mandelshtam, V. A.; Reisler, H. Reconstruction of Abel-Transformable Images: The Gaussian Basis-Set Expansion Abel Transform Method. *Rev. Sci. Instrum.* **2002**, *73*, 2634–2642.

(13) Hepp, M.; Herman, M. Weak Combination Bands in the 3-μm Region of Ethane. *J. Mol. Spectrosc.* **1999**, *197*, 56–63.

(14) Dang-Nhu, M.; Pine, A. S.; Lafferty, W. J. Intensities in the ν_5, ν_7 and $\nu_8 + \nu_{11}$ Bands of Ethane (C_2H_6). *Can. J. Phys.* **1984**, *62*, 512–519.

(15) Pine, A. S.; Lafferty, W. J. Torsional Splittings and Assignments of the Doppler-Limited Spectrum of Ethane in the C-H Stretching Region. *J. Res. Natl. Bur. Stand.* **1982**, *87*, 237–256.

(16) Western, C. M.; Billinghurst, B. E. Automatic and Semi-Automatic Assignment and Fitting of Spectra with PGOPHER. *Phys. Chem. Chem. Phys.* **2019**, *21*, 13986–13999.

(17) Gomez, L. F.; Sliter, R.; Skvortsov, D.; Hoshina, H.; Douberly, G. E.; Vilesov, A. F. Infrared Spectra in the 3 μm Region of Ethane and Ethane Clusters in Helium Droplets. *J. Phys. Chem. A* **2013**, *117*, 13648–13653.

(18) Wen, B.; Meyer, H. The Near IR Spectrum of the NO($X\Pi^2$)–CH_4 Complex. *J. Chem. Phys.* **2009**, *131*, 034304.

(19) *Constants of Diatomic Molecules in NIST Chemistry WebBook, NIST Standard Reference Database Number 69*; National Institute of Standards and Technology: Gaithersburg MD, 20899, 2023.

(20) Liu, J. Rotational and Fine Structure of Open-Shell Molecules in Nearly Degenerate Electronic States. *J. Chem. Phys.* **2018**, *148*, 124112.

(21) Beswick, J. A.; Jortner, J. Intramolecular Dynamics of van der Waals Molecules. In *Advances in Chemical Physics*; John Wiley & Sons, Ltd, 1981; pp 363–506.

(22) Ewing, G. E. Selection Rules for Vibrational Energy Transfer: Vibrational Predissociation of van der Waals Molecules. *J. Phys. Chem.* **1987**, *91*, 4662–4671.

(23) Andresen, P.; Rothe, E. W. Analysis of Chemical-Dynamics Via Λ-Doubling - Directed Lobes in Product Molecules and Transition States. *J Chem Phys* **1985**, *82*, 3634–3640.